Elastic Wave Propagation in Variable Media using a Discontinuous Galerkin Method

Thomas M. Smith, S. Scott Collis, Curtis C. Ober, James R. Overfelt, & Hans F. Schwaiger, Sandia National Laboratories

SUMMARY

Motivated by the needs of seismic inversion and building on our prior experience for fluid-dynamics systems, we present a high-order discontinuous Galerkin (DG) Runge-Kutta method applied to isotropic, linearized elasto-dynamics. Unlike other DG methods recently presented in the literature, our method allows for inhomogeneous material variations within each element that enables representation of realistic earth models — a feature critical for future use in seismic inversion. Likewise, our method supports curved elements and hybrid meshes that include both simplicial and nonsimplicial elements. We demonstrate the capabilities of this method through a series of numerical experiments including hybrid mesh discretizations of the Marmousi2 model as well as a modified Marmousi2 model with a oscillatory ocean bottom that is exactly captured by our discretization.

INTRODUCTION

Full waveform seismic inversion demands flexible numerical methods that can accurately handle strong inhomogeneities in subsurface medium parameters. Building on our prior experience using discontinuous Galerkin (DG) methods for optimal control of nonlinear fluid systems (Chen and Collis, 2004, 2008), our research team is investigating the potential of discontinuous Galerkin (DG) methods for time-domain full-waveform inversion. A companion abstract, (Collis et al., 2010), demonstrates the ability of DG methods to effectively perform acoustic inversion using both structured and unstructured grids along with local polynomial refinement. In that work, we take advantage of the fact that the partial differential equations governing acoustic wave propagation can be written in conservation form thereby allowing for arbitrary earth model variations within each element.

Unfortunately, the equations for linearized, isotropic elasto-dynamics are not readily cast in conservation form. However, DG methods have, nevertheless, been recently applied to seismic modeling by Dumbser, Käser and colleagues with a thorough series of papers (Dumbser and Käser, 2006; Käser and Dumbser, 2006; Käser et al., 2007; Dumbser et al., 2007b; Käser et al., 2010) documenting various aspects of their DG implementation combined with a Taylor-series time-integration technique. In these papers, the authors apply discontinuous Galerkin directly to the non-conservative equations of isotropic, linear elasticity (even including the effects of attenuation (Käser et al., 2007) and poroelasticity (de la Puente, 2008)). In so doing, they restrict their formulation to element-wise constant media representations on simplicial meshes that allows them to utilize a quadrature-free (Atkins and Shu, 1997) or, equivalently, nodal DG method (Hesthaven and Warburton, 2008). Such methods are well-known in the fluid-dynamics, aeroacoustics, and electromagnetics communities and are particularly appealing for linear transport equations within constant or piecewise constant materials. When applicable, these nodal DG methods can lead to very efficient numerical implementations (Warburton, 2008).

The work of Käser, Dumbser and colleagues has done an excellent job of showcasing the potential of nodal DG methods for homogeneous and nearly homogeneous earth models (see, *e.g.*, the simplified SEG Salt model shown in Käser et al. 2010). However, the restriction to piecewise constant media parameters is a major limitation in accurately representing realistic earth models since the element size required to capture the media variations would likely be much smaller than that required to accurately represent the wave field – potentially nullifying any computational advantage of the nodal DG formulation. For this reason, Dumbser et al. (2007a) have recently investigated high-order finite-volume methods for which the cell size for the wave field (with high-order reconstruction) and media would both be small and of similar size to that used for time-domain finite difference methods. Unfortunately, Dumbser et al. (2007a) show that even high-order finite volume methods tend to lose the impressive accuracy engendered by DG formulations.

Since, our ultimate goal is to leverage the flexibility and accuracy of DG methods for use in seismic inversion, this abstract focuses on a different, so-called modal, DG formulation that has been used extensively in the past by the second author and collaborators in the context of nonlinear, fluid dynamics simulation and control (Collis, 2002a,b; Collis and Ghayour, 2003; Chen and Collis, 2004, 2008). A modal DG method presents a number of potential advantages including the ability to support variable media within each element, curved element sides to better capture topology and geological features, as well as support for non-simplicial (quadrilateral and hexahedral) elements. We recently reported simple verification studies for our DG implementation using manufactured solutions of the acoustic wave equation (Ober et al., 2009). Subsequently, the method has been validated in both 2d and 3d against reference solutions and time-domain finite-difference codes for both acoustic and elastic physics. Due to space limitations, these studies are not reported here but will be summarized in the associated presentation.

This abstract proceeds as follows. The next section introduces the equations for linear elastodynamics including a brief description of our DG numerical formulation. This is followed by numerical results that demonstrate the flexibility in how earth models are parameterized, show the impact of choosing different earth model representations, highlight the flexibility in modeling complex geometric features, and illustrate the advantage of using an unstructured mesh to capture complex features within an elastic media.

NUMERICAL METHOD

The equations describing wave propagation in an isotropic, linear-elastic media (LeVeque, 2002) are a non-conservative, hyperbolic initial-value problem. In vector form, they are

$$\mathbf{U}_{,t} + \mathbf{A}_i \mathbf{U}_{,i} = \mathbf{S} \tag{1a}$$

$$\mathbf{U}(\mathbf{x},0) = \mathbf{U}_0(\mathbf{x}) \quad \text{at } t = 0 \tag{1b}$$

subject to appropriate boundary conditions, where $\mathbf{U}_0(\mathbf{x})$ is the initial condition, $\mathbf{S}$ is the source, $()_{,t}$ denotes differentiation with respect to time, $()_{,i}$ differentiation with respect to the ith Cartesian spatial component, and Einstein summation convention is used for repeated subscripts. For brevity, we present the formulation for two spatial dimensions. The extension to three-dimensions is straightforward and our actual implementation is dimension independent. The state vector is comprised of the dependent variables

$$\mathbf{U} = \left\{ \begin{array}{c} \sigma_{11} \\ \sigma_{22} \\ \sigma_{12} \\ v_1 \\ v_2 \end{array} \right\} \tag{2}$$

where the flux Jacobian is defined as

$$\mathbf{A}_i = -\begin{pmatrix} 0 & 0 & 0 & (\lambda+2\mu)\delta_{1i} & \lambda\delta_{2i} \\ 0 & 0 & 0 & \lambda\delta_{1i} & (\lambda+2\mu)\delta_{2i} \\ 0 & 0 & 0 & \mu\delta_{2i} & \mu\delta_{1i} \\ v\delta_{1i} & 0 & v\delta_{2i} & 0 & 0 \\ 0 & v\delta_{2i} & v\delta_{1i} & 0 & 0 \end{pmatrix} \tag{3}$$

and the flux vector in the ith-direction is $\mathbf{F}_i = \mathbf{A}_i \mathbf{U}$.

In these expressions, $\sigma_{ij} = \sigma_{ji}$ is the stress tensor, v_i is the particle velocity vector, and δ_{ij} is the Kronecker delta. The three media parameters are: Lame's first parameter, λ; Lame's second parameter (shear modulus), μ; and the specific volume, v. These are related to the compressive wave speed, c_p; shear wave speed, c_s; and mass density, ρ by $\lambda = \rho(c_p^2 - 2c_s^2)$, $\mu = \rho c_s^2$ and $v = 1/\rho$.

Equations (1) are solved on the spatial domain Ω subject to appropriate boundary conditions on $\Gamma \equiv \partial\Omega$. The domain is partitioned into N_{el} sub-domains Ω_e. We use the DG method to discretize in space leading to a system of ordinary differential equations in time. The DG formulation begins by seeking solutions $\mathbf{U} \in \mathscr{U}$ on each element, where $\mathscr{U}$ is an appropriate function space, and requiring that the residual be zero when integrated against the weighting functions $\mathbf{W} \in \mathscr{U}$. Starting from the strong-form (1a), taking the inner-product with the weighting function and integrating over an arbitrary element, e, leads to

$$\int_{\Omega_e} \mathbf{W} \cdot (\mathbf{U}_{,t} + \mathbf{A}_i \mathbf{U}_{,i} - \mathbf{S})\, d\Omega_e = 0. \tag{4}$$

We require that the flux Jacobians $\mathbf{A}_i$, which are a function of medium parameters, have sufficient smoothness *within each element* so that we can integrate by parts (however, media properties can have jumps on inter-element interfaces)

$$\int_{\Omega_e} \mathbf{W} \cdot (\mathbf{U}_{,t} - \mathbf{S}) - (\mathbf{W} \cdot \mathbf{A}_i)_{,i} \mathbf{U})\, d\Omega_e + \int_{\Gamma_e} \mathbf{W} \cdot \mathbf{F}_n\, d\Gamma_e = 0 \tag{5}$$

where $\mathbf{F}_n = \mathbf{F}_i n_i$ is the flux in the direction of the outward pointing unit-vector normal to the boundary. Replacing $\mathbf{F}_n(\mathbf{U})$ with a numerical flux $\hat{\mathbf{F}}_n(\mathbf{U}^e, \mathbf{U}^f)$, integrating by parts, and summing over all elements leads to our discontinuous Galerkin weak form

$$\sum_{e=0}^{N_{el}} \int_{\Omega_e} \mathbf{W} \cdot \left(\mathbf{U}_{,t} + \mathbf{A}_i \mathbf{U}_{,i} - \mathbf{S}\right) d\Omega_e + \sum_{e=0}^{N_{el}} \int_{\Gamma_e} \mathbf{W} \cdot \left(\hat{\mathbf{F}}_n(\mathbf{U}^e, \mathbf{U}^f) - \mathbf{F}_n(\mathbf{U})\right) d\Gamma_e = 0. \tag{6}$$

The numerical flux $\hat{\mathbf{F}}_n(\mathbf{U}^e, \mathbf{U}^f)$ plays the important role of propagating information from one element to another where $\mathbf{U}^e$ denotes the state interior to element e and $\mathbf{U}^f$ is the state on the element adjacent to element e at each point on Γ_e. The properties of the numerical flux are essential to ensure stability of the overall numerical method and the interested reader should consult (Cockburn, 1999; Cockburn et al., 2000; Hesthaven and Warburton, 2008; Toro, 1999). For discretization of conservation laws, the flux leaving one element is equal (but opposite in sign) to the flux entering the neighboring element. Therefore, the flux can be computed once at an element interface, negated and assigned to the neighboring element flux for that particular interface. However, for non-conservative systems such as linear elasticity, the flux at element boundaries must be computed separately in each element. For the studies presented here, we use Steger-Warming (SW) flux-vector splitting (Steger and Warming, 1981) which can be shown to be an exact Riemann solver for the linear system of equations considered here (Toro, 1999).

The boundary $\Gamma \equiv \partial\Omega$ is partitioned into free-surface, Γ_{fs} and non-reflecting Γ_{nr} regions and boundary conditions are enforced through the numerical flux by prescribing the external state $\mathbf{U}^f$. On the free-surface, the external state is set to the internal state but with components of the boundary normal stress vector negated. A non-reflecting condition is approximated by setting the external state to zero and adding a sponge-type (Grosch and Orszag, 1977) source term that damps wavefield variables near the non-reflecting boundary. A point explosion source is modeled by adding a Dirac delta function at the source location to the right hand side of the normal stress equations with the time variation given by the integral of a Ricker wavelet with peak frequency of 9.5 Hz and a time delay of 0.2 s.

To complete the spatial discretization, we approximate the function space $\mathscr{U}^h \approx \mathscr{U}$ using tensor products of orthonormal polynomials of order p defined on the master element. Integrals are evaluated using Gauss quadrature rules (Karniadakis and Sherwin, 1999) where the physical space element is mapped to the master element, in general, using an isoparametric mapping. The implementation is simplified for affine and simplicial straight-sided elements which have constant Jacobian mappings. Quadrilateral and hexahedral elements use tensor products of Legendre polynomials and simplicial elements (triangles and tetrahedra) use the orthonormal Dubiner polynomial basis (Karniadakis and Sherwin, 1999). While modal implementations have greater computational complexity than

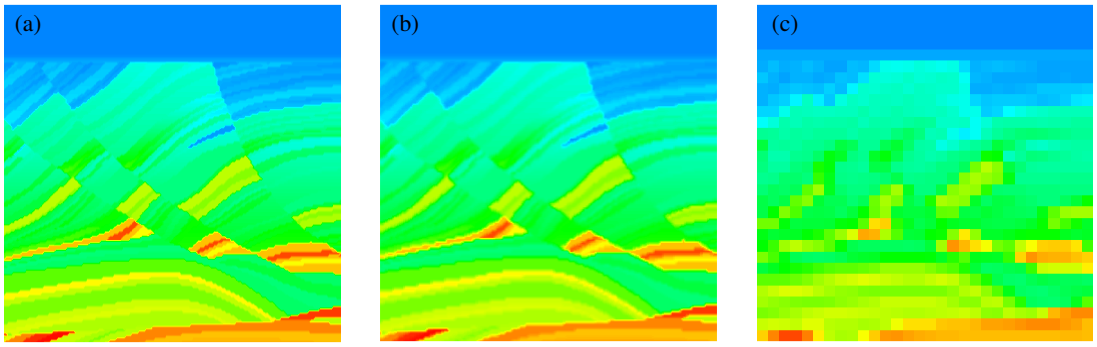

Figure 1: Comparison of earth model representations: (a) 20 m uniform sampling, (b) $p = 8$ DG representation on a $h = 100$m mesh, and (c) $p = 0$ DG representation on an $h = 100$ m mesh.

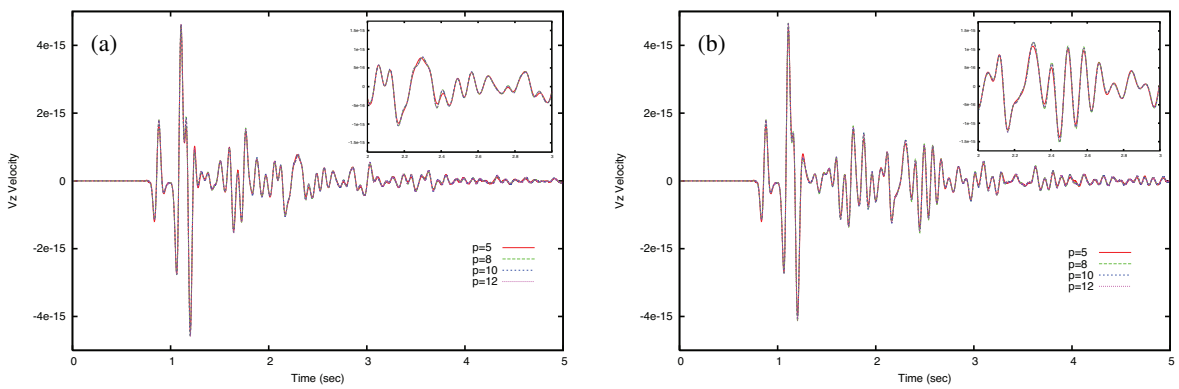

Figure 2: Traces of vertical velocity for DG simulations using (a) variable media and (b) piecewise constant media representations for different wavefield polynomial orders.

nodal implementations (Hesthaven and Warburton, 2008), they readily allow for variable media within the elements as long as spatial integrals are accurately computed. Our implementation also allows both the polynomial order, p, and quadrature order, q, to be varied element-by-element to better represent complex geological formations. With the exception of curved-sided elements, the use of orthogonal polynomial representations leads to identity mass matrices enabling efficient explicit time advancement. Curved elements require the solution of a local mass-matrix that is factored during setup and back solved on each time step. Our implementation supports a wide range of both explicit and implicit time advancement methods. However, for the cases presented here, we used a three-stage, third-order accurate Runge-Kutta method (Shu, 1988).

RESULTS

This section presents DG simulations for linear elasticity using the Marmousi2 earth model (Martin et al., 2006) that describes the elastic properties (ρ, c_p, c_s) of a geologically complex sea bed below a 500 m deep ocean layer. To provide an accurate model of the high-contrast interface between water and rock, all meshes used herein are designed to capture the ocean-bottom interface at an inter-element boundary. The seismic source is located 100 m below the water surface and a representative receiver is located 10 m below the surface and 1000 m to the left of the source.

Medium Representation

Figure 1 presents three representations of c_p on a 3000 m square window of the Marmousi2 model starting at $x, z = 8500, 0$ m. Figure 1(a) shows a 20 m uniform down sampling of the original 1.25 m Marmousi2 model and corresponds to the representation typically used in time-domain finite-difference methods at this frequency. Figure 1(b) shows a DG representation using our variable media capability. The DG mesh consists of a 30 by 30 array of 100 m square quadrilateral elements with $p = 8$ polynomial representation that was selected to give adequate wave field accuracy at this frequency. The 20 m down sampled Marmousi2 model is then linearly interpolated on the DG quadrature mesh leading to a model representation that is similar in quality to that used in finite-difference methods. In contrast, Figure 1(c) shows an element-wise constant medium representation of the type required to use quadrature-free DG (*e.g.*, Käser and Dumbser (2006)). The piecewise constant representation is unable to represent this complex geology and may be inadequate in the context of inversion.

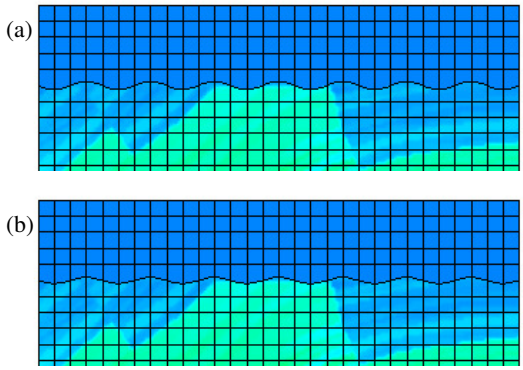

Figure 3: Compressional wave speed, c_p for a hilly representations of the Marmousi2 ocean bottom; (a) sine wave, (b) sawtooth. The amplitude is 25 m and the wave-length is 400 m.

To compare the differences in computed solutions, Figure 2 shows traces of vertical velocity at the receiver from DG simulations for both our (a) variable media formulation and for (b) piecewise constant media. In both cases, we used polynomial refinement of the wave field $p = 5, 8, 10, 12$ and the close-ups show that both solutions converge as polynomial order is increased. However, comparing the overall traces in frames (a) and (b) shows that the piecewise constant model converges to a different solution from the variable media case which provides a means to converge both the wave field and the model — a critical feature for inversion.

Ocean Bottom

To demonstrate the ability of our DG formulation to accurately represent complex topological features, we have applied a sinusoidal perturbation to simulate a "hilly" ocean bottom in the Marmousi2 model. We exactly capture this water-rock interface with an inter-element interface as shown in Figure 3(a). For comparison, a straight-sided approximation, such as might be used in a quadrature-free approach, is shown in Figure 3(b). Vertical velocity traces are presented in Figure 4 where differences suggest the importance of accurately representing topological features within the earth model.

Unstructured Mesh

Our final demonstration uses a fully unstructured mesh (see Figure 5(a)) of both triangular and non-affine quadrilateral elements that not only captures the ocean bottom but several major faults and high-contrast interfaces at inter-element boundaries. In so doing, the dynamics associated with these features are accurately represented by our DG numerical method. A snapshot of pressure is shown in Figure 5(b) demonstrating the ability of the method to surgically capture important interfaces at inter-element boundaries while also allowing variable media properties within elements for a high-fidelity representation of the earth model.

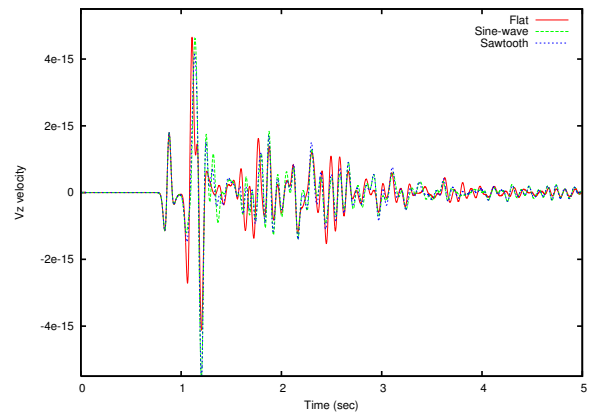

Figure 4: Traces of vertical velocity for flat, sine wave and sawtooth ocean bottom representations.

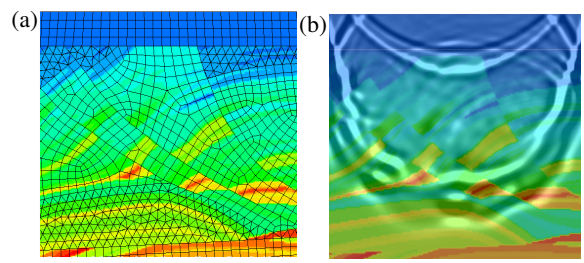

Figure 5: Unstructured Marmousi2: (a) close-up of the hybrid mesh with nominal mesh size of 100 m and contours of compressional wave speed c_p; (b) pressure wave field for unstructured mesh at t = 1.25 s.

CONCLUSIONS

A discontinuous Galerkin method for solving the equations of linear isotropic elasticity has been presented. The formulation is designed to accommodate variation of media parameters within elements, curved elements and unstructured heterogeneous meshes. We have demonstrated that each of these important features of the formulation can produce results that are significantly different from formulations that do not possess these capabilities suggesting that each of these capabilities may be important for effective full waveform inversion of elastic medium.

ACKNOWLEDGMENTS

This work has been supported by a Cooperative Research and Development Agreement (CRADA) between Sandia and an industrial partner. The authors would like to thank their colleague, David Aldridge, for advice and stimulating discussions regarding seismic simulation. Sandia is a multiprogram laboratory operated by Sandia Corporation, a Lockheed Martin Company, for the United States Department of Energy under contract DE-AC04-94AL85000.

REFERENCES

Atkins, H. L., and C.-W. Shu, 1997, Quadrature-free implementation of discontinuous Galerkin methods for hyperbolic equations: AIAA J., **36**, 775–782.

Chen, G., and S. S. Collis, 2004, Toward optimal control of aeroacoustic flows using discontinuous Galerkin discretizations: AIAA Paper 2004-0364.

———, 2008, Discontinuous Galerkin multi-model methods for optimal control of aeroacoustics: AIAA J., **46**, 1890–1899.

Cockburn, B., ed., 1999, Discontinuous Galerkin methods for convection-dominated problems, *in* High-order methods for computational applications, Lecture Notes in Computational Science and Engineering: Springer, 69–224.

Cockburn, B., G. Karniadakis, and C.-W. Shu, eds., 2000, Discontinuous Galerkin methods: Theory, computation, and applications: Springer.

Collis, S. S., 2002a, The DG/VMS method for unified turbulence simulation: AIAA Paper 2002-3124.

———, 2002b, Discontinuous Galerkin methods for turbulence simulation: Proceedings of the 2002 Center for Turbulence Research Summer Program, 155–167.

Collis, S. S., and K. Ghayour, 2003, Discontinuous Galerkin for compressible DNS: ASME Paper Number FEDSM2003-45632.

Collis, S. S., C. C. Ober, and B. van Bloemen Waanders, 2010, Unstructured discontinuous Galerkin for seismic inversion: SEG Technical Program Expanded Abstracts. (Submitted).

de la Puente, J., 2008, Seismic wave simulation for complex rheologies on unstructured meshes: PhD thesis, Ludwig-Maximilians-Universität.

Dumbser, M., and M. Käser, 2006, An arbitrary high-order discontinuous Galerkin method for elastic waves on unstructured meshes -II. The three-dimensional isotropic case: Geophysical Journal International, **167**, 319–336.

Dumbser, M., M. Käser, and J. de la Puente, 2007a, An arbitrary high-order finite volume schemes for seismic wave propagation on unstructured meshes in 2D and 3D: Geophysical Journal International, **171**, 665–694.

Dumbser, M., M. Käser, and E. F. Toro, 2007b, An arbitrary high-order discontinuous Galerkin method for elastic waves on unstructured meshes -V. Local time stepping and p-adaptivity: Geophysical Journal International, **171**, 695–717.

Grosch, C. E., and S. A. Orszag, 1977, Numerical solution of problems in unboundary regions: J. Comp. Phys., **25**, 273–296.

Hesthaven, J. S., and T. Warburton, 2008, Nodal discontinuous Galerkin methods: Alorithms, analysis and applications: Springer, volume **54** *of* Texts in Applied Mathematics.

Karniadakis, G. E., and S. J. Sherwin, 1999, Spectral/*hp* element methods for CFD: Oxford University Press.

Käser, M., and M. Dumbser, 2006, An arbitrary high-order discontinuous Galerkin method for elastic waves on unstructured meshes -I. The two-dimensional isotropic case with external source terms: Geophysical Journal International, **166**, 855–877.

Käser, M., M. Dumbser, J. de la Puente, and H. Igel, 2007, An arbitrary high-order discontinuous Galerkin method for elastic waves on unstructured meshes-III. Viscoelastic attenuation: Geophysical Journal International, **168**, 224–242.

Käser, M., C. Pelties, C. E. Castro, H. Djikpesse, and M. Prange, 2010, Wavefield modeling in exploration seismology using the discontinuous Galerkin finite-element method on HPC infrastructure: The Leading Edge, **29**, 76–85.

LeVeque, R., 2002, Finite Volume Methods for Hyperbolic Problems: Cambridge University Press, UK.

Martin, G. S., R. Wiley, and K. J. Marfurt, 2006, Marmousi2: An Elastic Upgrade for Marmousi: The Leading Edge, **25**, 156–166.

Ober, C. C., S. S. Collis, B. van Bloemen Waanders, and C. Marcinkovich, 2009, Method of manufactured solutions for the acoustic wave equation: SEG Technical Program Expanded Abstracts, **28**, 3615–3619.

Shu, C.-W., 1988, TVD time discretizations: SIAM J. Sci. Stat. Comp., **9**, 1073–1084.

Steger, J. L., and R. F. Warming, 1981, Flux Vector Splitting of the Inviscid Gasdynamics Equations with Application to Finite-Difference Methods: Journal of Computational Physics, **40**, 263–293.

Toro, E. F., 1999, Riemann solvers and numerical methods for fluid dynamics: Springer.

Warburton, T., 2008, Rocky mountain mathematics consortium summer 2008: Parallel numerical methods for partial differential equations. (http://www.caam.rice.edu/ timwar/RMMC/MIDG.html).